Radboud University Nijmegen

Faculty of Science

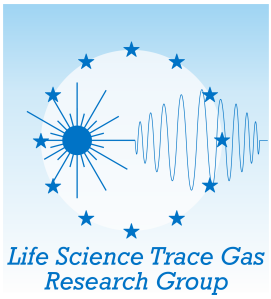

Wavelength modulation spectroscopy on traces of carbon monoxide using quantum cascade lasers

for medical diagnostics and plasma-catalytic conversion

Bachelor project Trace Gas Research group

Author:
Kees van Kempen
<ru@keesvankempen.nl>

Supervisor:
dr. Frans Harren

Second reader:
dr. Simona Cristescu

February 2020 – July 2021

Summary

Wavelength modulation spectroscopy (WMS) is a well-established technique for measuring trace gases (< 1 ppmv). By modulating the wavelength of a distributed feedback quantum cascade laser (DFB-QCL), wavelength modulation in the incident light results in intensity modulation in the detected light, which allows us to precisely measure trace gas concentrations. In this thesis, a look at the underlying theoretical principles is taken, and the main results for WMS are derived. The theoretic assumptions are tested and edge cases are discussed. The specific focus is the detection of traces of carbon monoxide (CO). Different approaches and approximations are discussed, and some are tested. A setup using discrete lock-in amplifiers is built, and then succeeded by a fully software-driven one. By using a homemade LabVIEW based signal generator and data processing combination, a detection limit of 20 ppbv of 100 mbar CO is reached. This is precise enough for most medical diagnostic uses (i.e. detection of exhaled CO; eCO, 1 ppmv to 5 ppmv), and offers good signal to noise ratios for detection in noisy environment (i.e. plasma). Finally, an outlook on the possible development of the technique is presented. By further reducing the amount of required devices, a compact and cheaper system can be built, thus making CO detection more accessible.

Contents

1 Introduction

Trace gases are gases of very small concentrations, ranging from a couple of parts per million volume (ppmv) to as little as a couple of parts per trillion volume (pptv). The term is often associated with atmospheric gases, but is also applied to occurrences of these tiny concentrations elsewhere. In this thesis, we will take a look at carbon monoxide. There are many different applications for trace gas detection of carbon monoxide (CO) in our current times. In biology and medical sciences, exhaled CO (eCO) is an important biomarker for a lot of diseases [1, 2]. The detection of concentrations of eCO provides us with more tools to assess a patient's health [3], and can offer a non-intrusive alternative to some invasive examinations [4]. Additionally, in search of ways to overcome

1. our dependence on petroleum for the production of bio-based chemicals,
2. the rising concentrations of greenhouse gases in the air,
3. and the lack of good mass energy storage methods,

the importance of CO_2 conversion methods is getting greater and greater. One promising but little researched technique for the conversion of CO_2 into value-added chemicals, is using plasma technology [5, 6]. Many of the possible plasma-catalytic processes to convert CO_2 into those value-added chemicals includes the generation of CO as an intermediate. Being able to measure the CO concentrations during such processes is therefore of uttermost importance. As the CO concentrations can be quite low and the conditions for measuring can be extremely noisy, we tend to laser spectroscopy as it has proven to achieve detection limits in the order of only a couple of parts per billion by volume (ppbv). Specifically, wavelength modulation spectroscopy (WMS) is used to overcome these harsh conditions. Moreover, other detection methods often rely on chemical processes to indirectly probe the concentration of CO and can therefore not be used to monitor chemical processes.

For my bachelor thesis, I have been looking into the WMS technique applied to traces of CO. By building an experiment, both physically and in software, an attempt is made to create a reproducible way to measure CO in trace gas concentrations and harsh conditions. Before doing so, the theoretical framework around this technique will be established.

The next subsections will introduce and quantify the notion of absorption of electromagnetic radiation by matter (1.1 and 1.3), the origin of this absorption in atoms and molecules (1.2), and the working principles of the light source used for the experiment (1.4). Finally, these concepts will be combined in the WMS technique in subsection 1.5.

1.1 Direct absorption

In order to say something about the composition of a gas, we require a way to identify and then distinguish different species of molecules in it. There are multiple properties that can be used for this distinction. Here we use the absorption of electromagnetic (EM) radiation. When electromagnetic waves pass through a molecule, part of the radiation is absorbed. The intensities of the radiation before and after passing the gas are compared

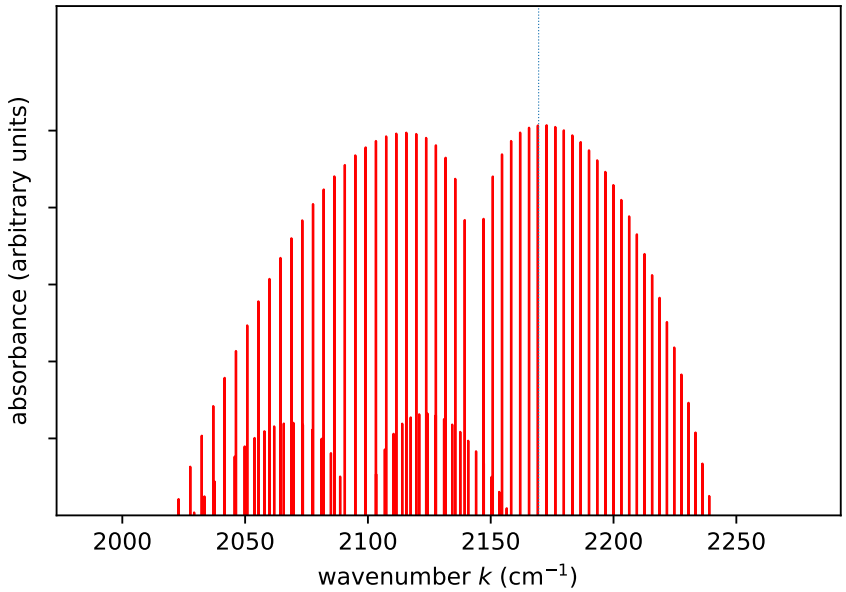

Figure 1: The spectrum of CO in the mid-infrared part of the EM spectrum in the picture is simulated using HITRAN data [7]. This window corresponds to the $\Delta v = 1$ band [8]. The line of interest, the CO R6 transition at 2169.50 cm^{-1}, is highlighted by the dotted vertical line.

and a difference in intensity is observed. The ratio between these intensities is called the transmittance T, which is defined as

$$T = \frac{I}{I_0},$$

where I_0 is the initial intensity and I is the transmitted intensity of the radiation. From the transmittance, we can calculate the absorbance A,

$$A = -\log_{10} T.$$

The absorbance can then be related to the concentration of the species of interest in the gas by the Lambert-Beer law,

$$A = \epsilon \ell c, \tag{1}$$

where ϵ is the absorptivity of the species of interest in the gas, ℓ is the length of the path through the gas along which the EM radiation travels, and c is the volumetric concentration of the species of interest in the gas. What allows us to make a distinction between different molecules, is that this absorptivity depends on the wavelength of the EM waves. For visible light, this is known as its color. This spectrum is like a fingerprint and differs from molecule to molecule. See figure 1 for an absorption spectrum of a pure CO gas in a part of the mid-infrared range of the EM spectrum.

As can be seen in this absorption spectrum of pure CO, this fingerprint consists of discrete lines corresponding to discrete wavelengths. These lines are due to the quantized nature of the energies of atomic orbits, as will be further investigated in the next section.

Knowledge of the shape and size of these absorption features allows us to quantify this fingerprint.

As is often the case, a sample consists of multiple gas species. The absorbance of some sample is then rewritten as a sum of the absorbances of the present species denoted by index i as

$$A(\omega) = \ell \sum_i \epsilon_i(\omega) c_i,$$

where we included the dependence on angular frequency ω[1], such that the transmitted intensity I can be expressed via

$$I(\omega) = I_0(\omega) T(\omega) = I_0(\omega) 10^{-\ell \sum_i \epsilon_i(\omega) c_i}.$$

A commonly used alternative measure for the degree of absorption is the attenuation cross-section σ. The absorptivity is related to the attenuation cross-section as

$$\epsilon_i(\omega) = \frac{N_A}{\ln 10} \sigma_i(\omega),$$

with N_A Avogadro's number, which gives a relation of the transmitted intensity I

$$I = I_0 e^{-\ell \sum_i \sigma_i(\omega) n_i}, \tag{2}$$

with n_i the number density of the attenuating species. Given, for all species in a sample, the absorption cross-sections $\sigma_i(\omega)$ and their line shapes, the composition of a sample can be reconstructed from the measured absorption spectrum. For many molecules, these cross-sections are known, and can be found in databases such as HITRAN [7]. These values are determined experimentally and through theory.

What is important to note, is that for trace gases, the measured intensities are often in the same order as the original intensities. This makes it hard to detect any absorption variations at all as noise is often larger and resolution coarser.

1.2 Rotational-vibrational transitions

In atomic spectroscopy, the absorption and emission of electromagnetic radiation, or photons, by atoms is considered. When a photon hits an atom, there is a chance of that photon being absorbed. The energy of the photon is transferred to the atom, and the atom gets excited into a higher energy state. These states $|\Psi\rangle$ are governed by the solutions to the Schrödinger equation for the system. A state $|\Psi\rangle$ is found as an eigenstate to the hamiltonian operator $\hat{H} = \hat{T} + \hat{V}$ of its kinetic and potential operators with the energy E its eigenvalue:

$$\hat{H} |\Psi\rangle = E |\Psi\rangle$$

The physical interpretation of these eigenstates are the possible orbits around a nucleus electrons can occupy. The electrons orbit around the nucleus in shells with discrete distances between these shells. Emission and absorption of photons correspond to the differences in energy levels between these shells. The change of energy of the system is given by

$$\Delta E = E_{\text{final}} - E_{\text{initial}}.$$

[1] As frequency ν and angular frequency $\omega = 2\pi\nu$ are very similar, those terms will be used interchangeably throughout this thesis.

For negative ΔE, energy leaves the system by emitting a photon with energy

$$h\nu = |\Delta E|,$$

where h is Planck's constant and ν is the frequency of the photon, which can also be expressed in terms of its wavelength ($\lambda = \frac{c}{\nu}$) or wavenumber ($k = \frac{1}{\lambda} = \frac{\nu}{c}$). If ΔE is positive, a photon with equal energy is absorbed. As this transition is only possible in fixed discrete steps, only photons with certain energies can be exchanged. This translates to the discrete lines in the absorption spectrum.

Molecules are more complex. They consist of multiple nuclei and electrons and can be in a larger variety of states. The energy levels of those states are not only determined by the electronic structure, but also by the vibrations and rotations between the atoms. An illustration of the energy levels of those states is displayed in figure 2. Again, these states are eigenstates to the Schrödinger equation for the system, this time of multiple atoms. Solutions to this Schrödinger equation are hard to find. Therefore, a common approximation is to treat the motion of the electrons and the nuclei separately, which is justified by the great difference in their masses. This is called the Born-Oppenheimer approximation. The molecular state structure is then made up of an electronic, and a rotational-vibrational part, which both affect the energy of the state. By first treating the nucleus as a rigid object having constant internuclear distance R, the solutions for the electronic states can be found. The effect of the ro-vibrational structure is regarded as a perturbation on the electronic structure. By allowing the internuclear distance R to vary, vibrational and rotational parts of the state are established. [9, p.357–381]

Going back to the formal notation of the eigenstates, quantum numbers can be assigned to each part of the structure. The largest contribution to the energy comes from the electronic structure, and is given by E_n^{el} for principal quantum number n. After the electronic contribution, the effect of the vibration is the greatest and we find $E'(v)$ as function of the quantum number v. The smallest effect comes from the vibrational structure, given by $E'(J)$ as function of the total orbital angular momentum J. The primes emphasize the fact that they are perturbation results. The energetic state of a molecule can then be captured by its quantum numbers as $|n\Lambda vJ\rangle$, including the projection of the orbital quantum number along the internuclear axis, Λ. This projection can be ignored for the energy levels, as it does not contribute to them.

In molecular spectroscopy, transitions between these molecular states are considered. A change of state $|n_i\Lambda_i v_i J_i\rangle \rightarrow |n_f\Lambda_f v_f J_f\rangle$ corresponds to the absorption or emission of electromagnetic radiation of energy

$$h\nu = |\Delta E| = |E_f - E_i|.$$

Again, as these energy levels are discrete, the transitions are as well. For most low energy experiments, the molecules stay in the electronic ground state, so changes in n are not considered. For the ro-vibrational spectrum, we just look at changes in v and J. However, not all those changes of state are allowed. Conservation of angular momentum and symmetry also need to be taken into consideration. From the conservation rules, selection rules for the transitions are derived: $\Delta J = 0, \pm 1$ and $\Delta v = \pm 1, \pm 2, \ldots$. These transitions are grouped into branches, of which in diatomical molecules due to the selection rules, only two are observed: the R-branch for $\Delta J = +1$ and the P-branch for $\Delta J = -1$. The Q-branch for $\Delta J = 0$ is negligible in most diatomic molecules. [10, p.43–52]

Referring back to figure 1, this part of the spectrum corresponds to the $\Delta v = \pm 1$ band, and a distinction between the P-branch on the left and the R-branch on the right of

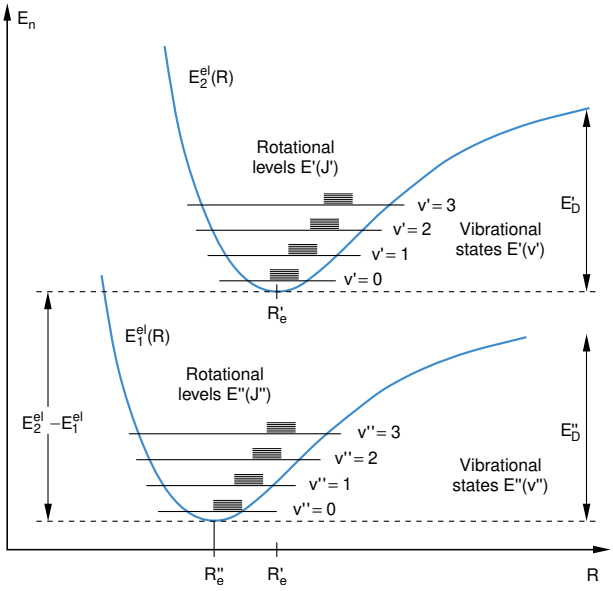

Figure 2: Molecular states can be decomposed into an electrical (E_n^{el}), a vibrational ($E(v)$) and a rotational ($E(J)$) part. [9, figure 9.52]

the 2040 cm^{-1} wavenumber can be made. In the performed WMS, only the CO R6 transition of wavenumber 2169.50 cm^{-1} is considered, as overlap with transitions of other molecules in the gas (H_2O, CO_2) is minimal (see figure 3) [1, 11], and the used light source is limited to this range.

1.3 Line shape functions

A last but not unimportant notion on absorption is that of the line shape.[12, p.13] In the previous section, the cross-section $\sigma(\omega)$ of absorption features was briefly mentioned. In this section, we found that emitted and absorbed photons are of discrete energies, determined by the structure of the atoms or molecules. Observed lines are, however, not infinitely sharp: the lines are broadened. What may look like sharp lines in, for example, figure 1, are actually mountains around a central energy. Due to effects like the uncertainty principle, the velocity of particles, pressure, and other parameters, the lines are broadened and we observe line shapes. [12, paragraphs 2.1–2.3]

These line shapes can be described by different functions, depending on the conditions and most notable broadening effects. Most common are the Gaussian and Lorentzian line shape functions, and their combination, the Voigt function. These functions are normalized, that is, the area under the curve equals one, as the total integrated absorption cross-section remains constant.

The first of three types of broadening is lifetime broadening. Due to the uncertainty of energy states, this molecule aspecific effect results broadening of the absorption line. This homogeneous broadening effect results in a Lorentzian line shape function

$$g(\nu_0, \nu) := \frac{2/(\pi\Delta\nu)}{1 + [2(\nu - \nu_0)/\Delta\nu]^2},$$

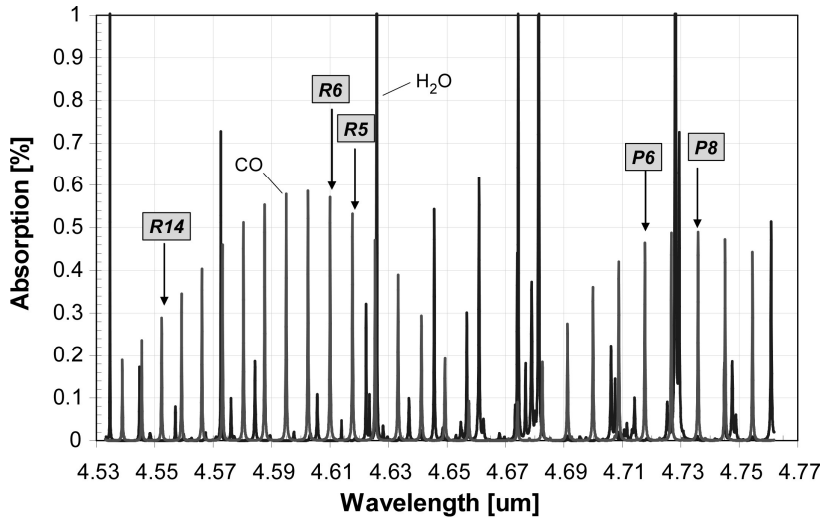

Figure 3: The spectrum displays the possible interference of H_2O (in black) to the absorption features of CO (in gray) near the R6 transition. It was simulated for the selection of a feature for a CO sensor in [11] (using HITRAN with 1 ppmv *CO at* 1 atm, 296 K *and a* 1 meter *pathlength).*

which is a function proportional to the absorption cross-section at frequency ν around center frequency ν_0. The distribution around ν_0 is characterized by the full width at half maximum (FWHM) $\Delta\nu$. In the case of lifetime broadening, the equality $\Delta\nu = \frac{1}{2\pi\tau}$ holds for the mean lifetime τ of an excited state. It is mostly visible if other broadening effects are small, at very low pressure and temperature.

The second mechanism that results in Lorentzian broadening, is that of interaction between molecules in a gas. This is called collision or pressure broadening. The FWHM $\Delta\nu$ is a function of partial pressures with linear constants depending on the interaction between molecular species and molecules of the same species.

The third type is Doppler broadening, a type of inhomogeneous broadening. In solids, this is mostly due to the presence of particles with different emission lines. In gases, this effect is usually dominant over homogeneous broadening, and is due to velocity of the molecules parallel to the light direction. This effect can be quantized with a Gaussian line shape function

$$g(\nu_0, \nu) := \frac{2}{\Delta\nu}\sqrt{\frac{\ln 2}{\pi}} e^{-[2(\nu-\nu_0)/\Delta\nu]^2 \ln 2}, \tag{3}$$

again of the same parameters as above. For inhomogeneous broadening, the FWHM $\Delta\nu$ can be expressed as

$$\Delta\nu = \frac{\nu_0}{c}\sqrt{\frac{8k_B T \ln 2}{M}},$$

with k_B the Boltzmann constant, T the temperature of the gas, atomic mass M, and the speed of light c.

For most measurement techniques, sharper lines are desired. This often means pressure is kept low to minimize collision broadening. In the case of (trace) gas absorption, the major effects are Doppler and collision broadening.

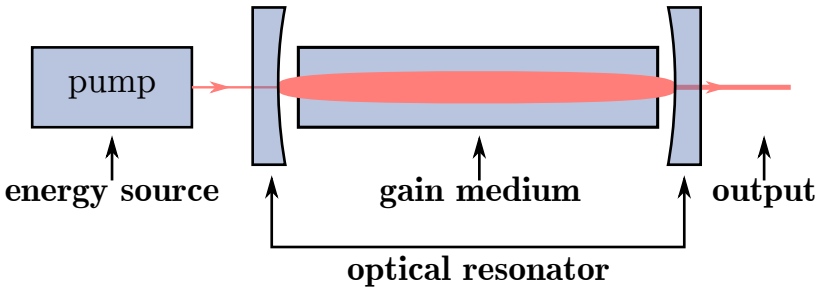

Figure 4: A schematic diagram of a typical laser is shown. The pump puts energy into the system. In the gain medium, photons are produced by a process of stimulated emission. This effect is amplified by the oscillation due to the resonator, producing more and more coherent photons. In a gas laser, for example, the optical resonator would consist of two mirrors, with on the left side an inlet and on the side a small outlet in the center.

1.4 Quantum cascade laser

As was seen in the previous subsections, the CO molecule can be recognized by its fingerprint in the mid-infrared region. In order to "see" the molecules, we therefore need a light source that emits EM radiation in that region. The light has to be predictable, and, for the WMS technique, it also has to be modulated. The logical way to go is with lasers, which luckily have been around for some decades.

A laser, originally an abbreviation for Light Amplification by Stimulated Emission of Radiation[2], is a monochromatic emitter of coherent electromagnetic radiation through the process of stimulated emission. Typically, a laser emits a tightly focused beam at a very narrow wavelength band. Although there are various types of lasers, they are all made up of three principal parts: an energy source, a gain medium, and some type of optical resonator. Before looking into the specific kind of laser used during my internship, we will first cover this general concept of a laser.

A schematic depiction of a typical laser is shown in figure 4. The energy source provides energy to the system. This process is called pumping. Electrons in the gain medium are excited into a higher energy state from which they can decay under the emission of a photon. In the process of spontaneous emission, these photons are produced in any random direction. Depending on the incident direction, the resonator feeds back the photon through the gain medium or absorbs it. It may or may not be desired that this reflection depends on the wavelength of the photon. When this photon hits an excited electron, the electron decays under the emission of a photon with the same wavelength, direction, and phase of the incident photon. This incident photon therefore stimulates the emission of another equivalent photon, and this new photon can do so, again. If enough electrons are in the excited state, and there are enough photons to stimulate the decay, there is a point at which the stimulated emission dominates the spontaneous emission, and we say the laser *lases*. The result is an intense, coherent beam of light. Naturally, however, the distribution of electrons in the lower and higher energetic states is such that the lower states are more heavily populated. In our laser system, this is not the case. The situation of having more electrons in an excited state than in their ground state, is called population inversion. [12]

[2]Fun fact of the year is that Oscillation fitted better than Amplification [12, p.1, footnote 1].

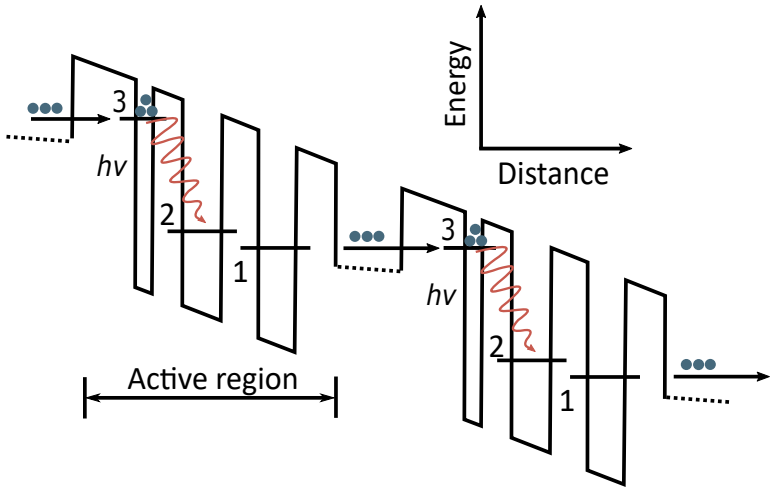

Figure 5: The energy levels of a quantum cascade laser are shown for two stages (by the black lines). The electrons (blue-green) tunnel from the higher to the lower states under the emission of a photon of energy equal to the difference between the energy states. [15, p.554, figure 1.A]

There are numerous types of mid-infrared lasers as are compared in [13, p.10–15]. Due to its tunability, compactness, and its performance even at room temperature, the quantum cascade laser (QCL) is chosen as the light source for these experiments. First, we will take a look at how the laser works, and then we will see how the emission can be modulated.

A QCL is a semiconductor laser. In most semiconductor lasers, radiation is emitted as a result of electron-hole recombination between the valence and conduction band (interband transitions). The energy of the radiation then depends on the band gap of the material. In QCLs, however, the radiation originates from the tunneling of electrons between states within a system of quantum wells confined to the valence band or the conduction band (intraband or intersubband transitions). The thicknesses of the quantum wells and the barriers determine the energies of these transitions. The resulting emission is therefore a consequence of design, not only of the materials used. A schematic representation of the energy levels is displayed in figure 5. [14, paragraph 2.3]

Figure 6 shows the composition of a QCL. A supply voltage is applied over the top and bottoms contacts, creating a potential over the active region. The structure of the active region of a typical (simplified) QCL consists of a composition of stages with each three energy levels. Electrons are injected in some upper energy level. By tunneling from level 3 to level 2, a photon of a certain energy is emitted. After this step, by fast tunneling from levels 2 to 1, the electron reaches energy level 3 for the next stage. The structure is made such that the decay from levels 2 to 1 is far more probable than the decay from levels 3 to 2. In this way, population inversion is achieved: there are more electrons in the higher level 3 than in level 2. This is desired as then the spontaneous emission is minimized. To keep a good supply of highest energy electrons, a current from the power supply will flow. This is called the injection current.

When many of these stages are combined, a cascading effect occurs, and multiple photons are emitted per injected electron. Depending on the purpose of the laser, the difference

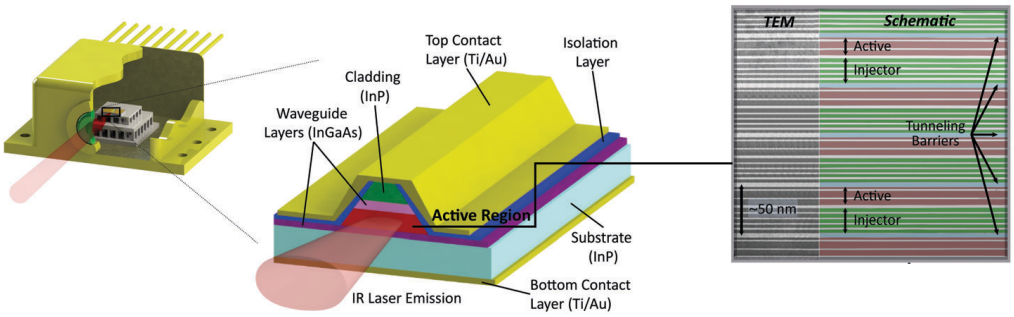

Figure 6: The QCL is driven by a voltage applied over the top and bottom contacts. At a sufficient voltage, a potential gradient arises over the grating structure. Electrons populate various potential wells. By tuning the thicknesses of the semiconductor layers, the energy levels can be tuned. A waveguide of some sorts contains the emission. [16]

in energy between levels 3 and 2 is the same for all stages, thus generating a laser beam of one wavelength (single-mode), or these differences vary, generating a spectrum of multiple wavelengths (multi-mode). For most spectroscopy applications, single-mode operation of a QCL is required, as is for the WMS technique.

In order to stimulate the decay from levels 3 to 2, the photons interact with the excited electrons, thus resulting in stimulated emission. Emitted photons are to be fed back through the gain medium, the active region. For this optical feedback, a Bragg grating is used. A periodic structure diffracts the light. The angle of diffraction depends on the wavelength of the photons and the physical dimensions of the grating. QCLs using this kind of feedback are called distributed feedback QCLs (DFB-QCLs). The grating dimensions are affected by changes in temperature by thermal expansion. A linear tuning coefficient of the center wavenumber (inverse wavelength) over the temperature $\Delta k/\Delta T = 1/(\Delta\lambda\Delta T)$ characterizes this effect. The QCL is kept at a constant average temperature by a heat sink to control this temperature.

There are two ways to change the emitted wavelength through temperature.[17] The first is by changing the temperature of the heat sink. This is a slow process and is used to change the average wavelength. The second method is to change the supply current. By increasing the supplied current, the power is increased, and the temperature of the grating is changed. The average temperature is still determined by the heat sink temperature, so the latter works only for a changing current. At a constant heat sink temperature, a linear tuning coefficient $\Delta k/\Delta P$ in wavenumber per unit power can be found through simulation or measurement. In the literature, this is often called injection current modulation. There is one catch, however. The emitted intensity is also increased with increasing supply current. Modulating the wavelength thus also yields simultaneous intensity modulation. An example of the wavelength and output power response of a DFB-QCL of the type of our interest, is displayed in figure 7. [13, p.21–26][14, p.20–23]

1.5 Wavelength modulation spectroscopy

In section 1.1, direct absorption was discussed. The Lambert-Beer law (equations (1) and (5)) was introduced, and the notion of direct absorption was thereby quantified. In section 1.2, the origin of these absorption features in atoms, and in particular, molecules was qualitatively explained. The existence of line shapes was explored in section 1.3.

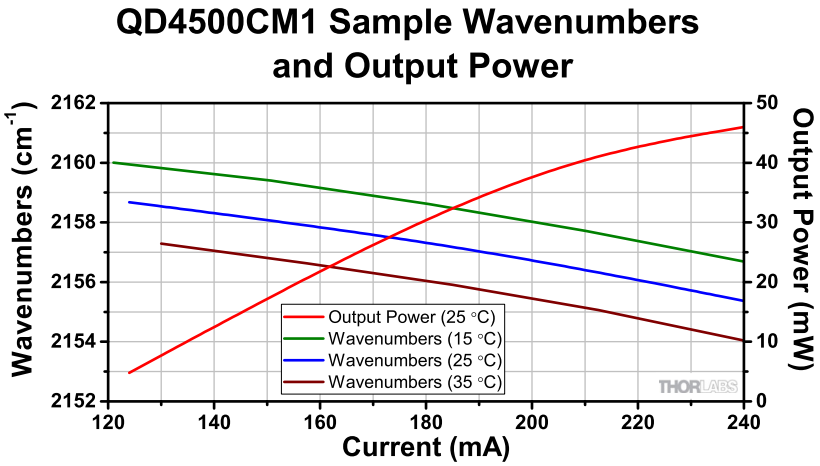

Figure 7: A graph of the QD4500CM1 center wavenumber and output power over the supplied current as supplied by Thorlabs is displayed for different temperatures of the heat sink. [18]

Then in section 1.4, the QCL was introduced and the ability to modulate its output wavelength and intensity was proposed and quantified. This seems enough to measure absorption due to a gas species. However, as this thesis is concerned with trace gases, the concentrations, and therefore the absorbances, are tiny. Noise is often larger than the desired signal. Furthermore, the absorption is just a fraction of the total measured signal. This section introduces a technique to try to eliminate this problem: wavelength modulation spectroscopy. By introducing a harmonic component to the wavelength of the laser light, the signal can be extracted from the noisy environment using lock-in amplification.

There are many sources of good information on wavelength modulation spectroscopy. All have their own angle, and so does the next subsection. Before continuing, let me note some good and popular literature on the technique. A discussion of the technique with some proper justification of approximations can be found in [19]. In [20], the authors present a practical implementation of calibration-free 2f/1f WMS in "harsh environments". A more rigorous derivation of the theory can be found in [21], for those that want to dig even deeper and look into utilizing higher order harmonics. All relevant approximations and derivatives will be discussed in the following paragraphs, taking great inspiration from mostly the first of these sources.

Consider an absorption feature of a gas molecule at a certain center wavelength with a QCL emitting light in the same wavelength region. As the light beam passes the gas, part of the light is absorbed, and the resulting intensity is measured. Now the wavelength of the QCL is modulated using a sine wave. This in turn modulates the wavelength of the light. Due to the line shape of the absorption feature, this wavelength modulation in the incident light results in an intensity modulation in the absorbed light. This effect is illustrated in figure 8. Due to the shape of the absorption line, the absorption is largest around the center wavelength ω_0 and slowly decays as the laser wavelength deviates further from it. By positioning the center wavelength of the laser such that $\omega_L = \omega_0$, the signal as plotted in the right graph of figure 8 is detected.

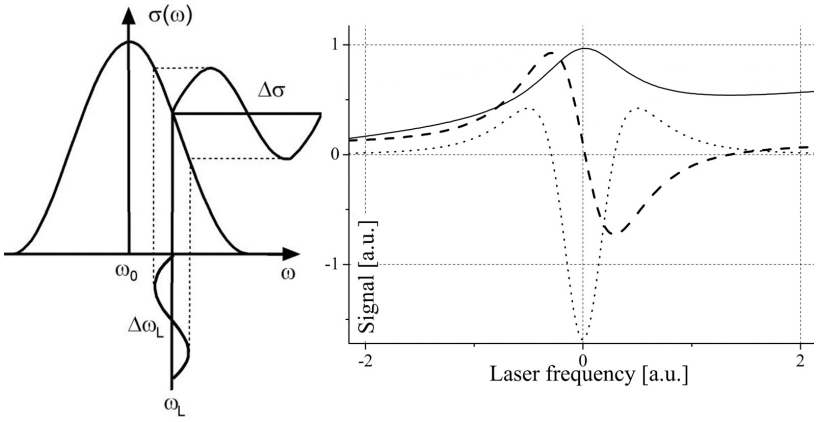

Figure 8: In the left panel, the translation from wavelength modulation in the incident light (horizontal axis) to a modulation in absorption cross-section (vertical axis) is illustrated. The resulting intensity modulation (and its first and second derivative, respectively the solid, dashed, and dotted lines) in the detected absorption is plotted in the right panel. [22, figure 3.7]

1.5.1 Quantitative model of a WMS experiment

Before looking at what can be measured, we will take a look at a theoretic description of the resulting intensity modulation in the detected signal. By shining a laser light of a single known wavelength through a gas sample, direct absorption can be measured by comparing the intensity to the situation in absence of this sample. Changing the wavelength of the laser light over time allows us to scan an absorption spectrum over a portion of the EM spectrum of the beam wavelength. If there is one absorption feature in this part of the EM spectrum, one absorption peak is detected, as can be observed as a valley on the rising slopes of the last graph in figure 9. For high concentrations and long paths, this could be enough to measure the absorption over time. In the case of trace gases, the figure is a little exaggerated. Most absorption features for gases with volumetric concentration in the order of parts-per-million, parts-per-billion, or even parts-per-trillion, cannot be measured this way due to noise. We therefore modulate the supply current by superimposing a sine wave of frequency ω_m. The resulting injection current can be quantified by summing the currents

$$j(t) = j_0 + j_{scan}(t) + j_{mod}(t).^3 \tag{4}$$

It is important that the rate of change by the modulation is way larger than the rate of change due to the scan. The current $j_0 + j_{scan}(t)$ should be approximately constant with respect to the timescale of the modulation $j_{mod}(t)$ for the following theory to apply. The goal of the scan is to always keep the absorption feature in frame. Due to, for example, temperature shifts, the wavelength of the laser light could vary, and a steady j_0 would not be enough to keep the average laser wavelength at the center wavelength of the absorption feature. In the following derivations, it is assumed this requirement is met.

The effect of the current modulation is a simultaneous wavelength and intensity modulation (WM and IM). The incident laser intensity $I_0(t)$ is modeled by

$$I_0(t) = \bar{I}_0\big[1 + i_0 \cos(\omega_m t + \psi_1) + i_2 \cos(2\omega_m t + \psi_2)\big], \tag{5}$$

[3] Using j instead of I or i for electrical currents as not to confuse them with the light intensities.

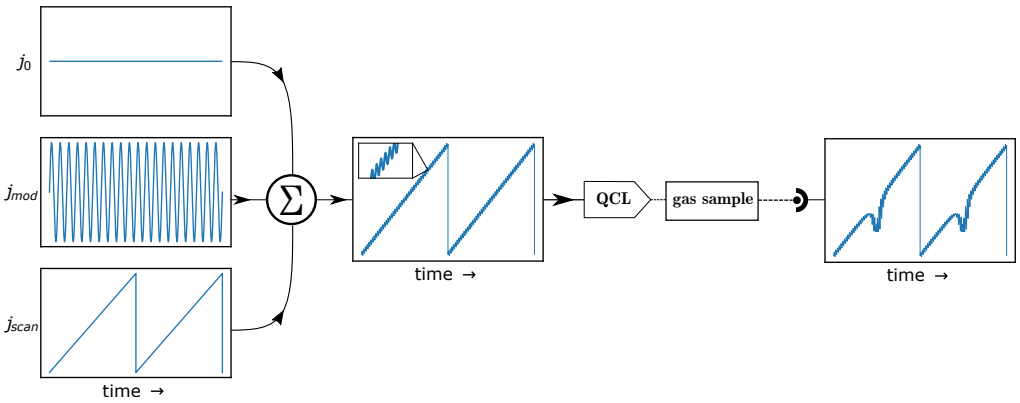

Figure 9: The injection current of the QCL is a mix of a DC signal j_0, a scanning j_{scan}, and a sine for modulation j_{mod}. The result is a wavelength but also intensity modulated scan. At half a period of the scan, the QCL emits at the frequency of the absorption feature of the species of interest.

with

- $\bar{I}_0$ the average laser intensity in the timescale of the modulation,
- i_0 and ψ_1 the relative intensity of the linear first order harmonic and its phase shift with respect to the injection current,
- i_2 and ψ_2 the relative intensity of the nonlinear second order harmonic and its phase shift with respect to the injection current.

This cosine is chosen instead of the sine to make the calculation of the Fourier series easier. Note that $\bar{I}_0$ and ω_L are still slowly varying due to the scanning current.

The frequency $\omega(t)$ is then modeled by

$$\omega(t) = \bar{\omega}_L + \Delta\omega_L \cos(\omega_m t), \tag{6}$$

with

- ω_L the center frequency of the laser light,
- $\Delta\omega_L$ the modulation amplitude of the laser light due to the injection current modulation.

Now this incident laser beam of intensity $I_0(t)$ and frequency $\omega(t)$ passes a single species gas sample. The frequency of the transmitted beam remains the same, but the intensity $I_t(t)$ changes as follows.

$$I_t(t) = I_0(t) \exp(-\ell\sigma(\omega(t))n) \tag{7}$$

$$= I_0(t) \exp\big[-\ell\sigma(\omega_L + \Delta\omega_L \cos(\omega_m t))n\big] \tag{8}$$

Knowledge of the absorption cross-section function $\sigma(\omega)$ is therefore needed. If the cell absorbance $a = \ell\sigma(\omega)n$ is small, that is, $a << 1$, the exponent can be simplified using a first-order Taylor series $\exp(-a) \approx 1 - a$.

$$I_t(t) \approx I_0(t)\big[1 - \ell\sigma(\omega_L + \Delta\omega_L \cos(\omega_m t))n\big] \tag{9}$$

If the intensity modulation is small, that is $i_0, i_2 << 1$, we also find

$$I_t(t) \approx \bar{I}_0\big[1 - \ell\sigma(\omega_L + \Delta\omega_L \cos(\omega_m t))n\big]. \tag{10}$$

This transmitted intensity can then be expressed in terms its harmonics by a Fourier series as

$$I_t(t) = \sum_{k=0}^{\infty} A_k(\omega_L)\cos(k\omega t). \tag{11}$$

With amplitudes for the individual harmonic components for $k > 0$ given by

$$A_k = \frac{1}{\pi}\int_{-\pi}^{\pi} \bar{I}_0\big[1 - \ell\sigma(\omega_L + \Delta\omega_L \cos(\omega_m t))n\big]\cos(k\theta)d\theta \tag{12}$$

$$= \frac{2\bar{I}_0\ell n}{\pi}\int_0^{\pi} -\sigma(\omega_L + \Delta\omega_L \cos(\omega_m t))\cos(k\theta)d\theta, \tag{13}$$

where the fact that $\cos(k\theta)$ is even is used, and $\theta = \omega t$ is substituted. In the case that modulation amplitude $\Delta\omega_L << \omega_L$, thus the modulation is small compared to the center wavelength, a Taylor expansion of $\sigma(\omega)$ around ω_L is used to arrive at the following expression for the integral we call Ξ.

$$\Xi := \int_0^{\pi} -\sigma(\omega_L + \Delta\omega_L \cos(\omega_m t))\cos(k\theta)d\theta \tag{14}$$

$$= \int_0^{\pi}\Big[-\sum_{N=0}^{\infty}\Big(\frac{d^N\sigma}{d\omega^N}\Big|_{\omega=\omega_L}\frac{[\Delta\omega_L\cos(\theta)]^N}{N!}\Big)\cos(k\theta)d\theta\Big] \tag{15}$$

The integral can be solved by considering the identity

$$\int_0^{\pi}\cos(\theta)^N \cdot \cos(k\theta)d\theta = \begin{cases} 2^{-k}\pi & \text{for } N = k \\ 0 & \text{for } N \neq k, \end{cases}$$

for $k, N \in \mathbb{N}$, which results in

$$\Xi = \int_0^{\pi} -\sigma(\omega_L + \Delta\omega_L \cos(\omega_m t))\cos(k\theta)d\theta \tag{16}$$

$$= \int_0^{\pi}\Big[-\sum_{N=0}^{\infty}\Big(\frac{d^N\sigma}{d\omega^N}\Big|_{\omega=\omega_L}\frac{[\Delta\omega_L\cos(\theta)]^N}{N!}\Big)\cos(k\theta)\Big]d\theta \tag{17}$$

$$= -\frac{d^k\sigma}{d\omega^k}\Big|_{\omega=\omega_L}\frac{2^{-k}\pi}{k!}. \tag{18}$$

Substituting the integral back into equation (12) returns

$$A_k = \frac{-2^{1-k}\bar{I}_0\ell n}{k!}(\Delta\omega_L)^k\frac{d^k\sigma}{d\omega^k}\Big|_{\omega=\omega_L}. \tag{19}$$

These harmonic amplitudes A_k are the core result of the WMS technique. They are useful for detecting species of low absorption as their values are directly proportional to the present concentration. In the next subsection, these amplitudes will be linked to practically detectable signals.

1.5.2 Lock-in detection

In the lock-in amplifier, the detected signal proportional to the intensity $I_t(t)$ is multiplied by either a sine or a cosine of frequency $k\omega$ ($k \in \mathbb{N}$). The result is two signals X and Y, which are proportional to respectively the in-phase amplitude and its quadrature ($+90°$ phase) amplitude. Taking the root of the sum of their squares gives us the total magnitude of the harmonic amplitude R, which is proportional to amplitudes A_k. If the signal is completely in phase, that is $Y = 0$, only X is required. This can be achieved by tuning ϕ_{ref} on the lock-in amplifier, but is not required, although it simplifies to mathematics a lot. For the k-th harmonic kf, we find at any time t

$$X_{kf}(t) = \frac{1}{\tau}\int_{t-\tau}^{t} I_t(s)\cdot\sin\left(k\omega s + \phi_{ref}\right)ds, \quad Y_{kf}(t) = \frac{1}{\tau}\int_{t-\tau}^{t} I_t(s)\cdot\cos\left(k\omega s + \phi_{ref}\right)ds. \tag{20}$$

Through the Fourier series expansion of $I_t(t)$, one can determine that for large τ, thus averaging the signal over many times the modulation time, $R_{kf} = \sqrt{X_{kf}^2 + Y_{kf}^2}$ will estimate $\frac{1}{2}V_L A_k$ [23], where V_L is the gain of the amplifier [24, chapter 3].

By measuring these harmonic amplitudes X and Y, or just R using a lock-in amplifier, a link between A_k and present concentration (number density n) can be made, if the optical path length ℓ and k-th derivative of the absorption cross-section $\sigma(\omega)$, which also depends on temperature T of the sample, are known. Measurement of A_k at a known concentration then allows us to find other concentrations using this method.

A while back, we made the assumption that $I_0(t) \approx \bar{I}_0$. By considering the 2f harmonic (A_2), the scanning part of the intensity modulation on the incident laser beam can be rid of, as its contribution will equal zero in and after the second derivative. The effect of the change of wavelength over the scan is visible, though. In figure 8, the graphs on the right are of the lock-in measured harmonics R. The solid line is the direct signal, the dashed line is the 1f signal, and the dotted line is of the 2f signal. In the direct signal, the effect of the scan is clearly visible. The mean absorption seems to rise over time due to this. The center wavelength can be found at the time the 1f signal crosses zero and the 2f signal is minimal. This is the point we are most interested in as only in this point $\omega_0 = \omega_L$. In the following, the symbols 1f and 2f are used to refer to the R values of respectively the 1f and 2f harmonic components as measured by the lock-in amplifier at the $\omega_0 = \omega_L$ point.

For the k-th, first, and second harmonic, the following expressions are found.

$$kf = R_{kf} = G_k\left|A_k\right| = G_k\frac{2^{1-k}\bar{I}_0\ell n}{k!}(\Delta\omega_L)^k\left|\frac{d^k\sigma}{d\omega^k}\right|_{\omega=\omega_L}\Bigg| \tag{21}$$

$$1f = R_{1f} = G_1\left|A_1\right| = G_1\bar{I}_0\ell n\Delta\omega_L\left|\frac{d\sigma}{d\omega}\right|_{\omega=\omega_L}\Bigg| \tag{22}$$

$$2f = R_{2f} = G_2\left|A_2\right| = G_2\frac{\bar{I}_0\ell n}{4}(\Delta\omega_L)^2\left|\frac{d^2\sigma}{d\omega^2}\right|_{\omega=\omega_L}\Bigg| \tag{23}$$

These provide a good linear relation of concentration n to the measured signal, as long as all previously covered conditions are met. Dependence on the temperature and pressure

of the gas is implied by the line shape function of the absorption feature. See section 1.3 for information on this dependence. The proportionality factor is equal to $\frac{1}{2}V_L$ as was mentioned before. In the following, the electro-optical gain of the system for measuring the k-th harmonic will be summarized by gain factor G_k, as they may differ between lock-in amplifiers but will be constant over time.

1.5.3 Intensity modulation

In the previous quantitative model, it was assumed intensity modulation was negligible ($i_0, i_2 << 1$). It turns out that we do need to consider changes to the laser intensity due to the injection current variations and other effects as to reach higher sensitivities ($<$ 1 ppmv). The superposition of the scanning current onto the injection current implies a constant change of the intensity of the laser. This effect would be visible in measurement of the original as a ramp, and of the 1f signal as a non-zero baseline. For higher harmonics, the measured signals are indeed zero baseline, which makes them ideal to look at small variations. Still, the intensity I_0 might be subject to changes due to modulation or even over time. Other effects, such as a wavelength dependent gain of the laser, could also be significant. There are multiply approaches for applying a correction to this [25]:

1. simultaneously measuring incident intensity using a parallel optical path without the gas sample;
2. finding a Fourier series description of the intensity modulation to express the incident intensity at $\omega_0 = \omega_L$;
3. finding a relation of the incident intensity using the 1f signal to normalize the higher harmonics.

The first option does not take into account the losses and fluctuations in the whole optical path of the primary beam, and is impractical in harsh environments [26]. The second option would involve measuring the parameters i_0, ψ_1, i_2 and ψ_2 from equation (5) at $\omega_L = \omega_0$ [20]. This usually done by simulation to fit these parameters to a measurement [27]. Determination of the intensity modulation in WMS using QCLs is thoroughly discussed in [26]. The last option is a little coarser, but as it covers most effects of intensity modulation that are harder to cover with the other methods (deflections, stray absorptions), it is a good option. Our focus will be on this last method.

For optically thin absorptions ($a = \ell\sigma(\omega)n < 0.05$), the effect of absorption is negligible in the 1f signal [26], and it can therefore be used as if it is a direct measurement of the incident laser intensity (similar to option one above). Equation (22) then gets replaced by

$$1f = R_{1f} \approx G_1 \bar{I}_0. \tag{24}$$

The resulting 1f-normalized 2f magnitude then becomes

$$2f/1f \approx \frac{G_2\,|A_2|}{G_1 \bar{I}_0} = \frac{G_2}{G_1}\frac{\ell n}{4}(\Delta\omega_L)^2 \left| \left. \frac{d^2\sigma}{d\omega^2} \right|_{\omega=\omega_L} \right|. \tag{25}$$

Characterization of the system by relating $2f/1f$ proportional to n is now possible.

1.5.4 Large modulation depths

In equation (12), the assumption of a small modulation regime ($\Delta\omega_L << \omega_0$) is made. This allows us to look at the k-th harmonic signal as being proportional to the k-th derivative of the line shape $\sigma(\omega)$. In practice, however, small modulation results in too small a signal. By increasing the modulation depth (or modulation index) $\Delta\omega_L$ to roughly the width of the absorption feature, better signals are acquired [19]. For the first and second harmonics, the proportionality to their respective derivatives still roughly remains.

2 Experimental setup

For a large part, the setup is taken from [1]. A photo of the full setup is shown in figure 10. A schematic of the setup is shown in figure 12. The QCL is a continuous-wave DFB-QCL (M905I, Maxion Technologies) as described in section 1.4. The QCL chip and enclosure can be seen in figure 11. Over the course of the internship, the QCL had to be repaired, and its characteristics have changed with that. This means that the optical output power at the desired wavelength (around the R6 transition of CO) has been reduced from 20 mW to 200 µW. The setup was adapted to this change. Coincidentally, another lock-in amplifier arrived at the moment the QCL was repaired, thus a change of setup was no hassle. Finally, the setup was compacted by performing the signal generation and lock-in amplification in LabVIEW. The initial setup is described in the first subsection, the adaption to the extra lock-in amplifier and the lower optical power is discussed in the second subsection, and the final conversion to a wholly LabVIEW steered setup is described in the third.

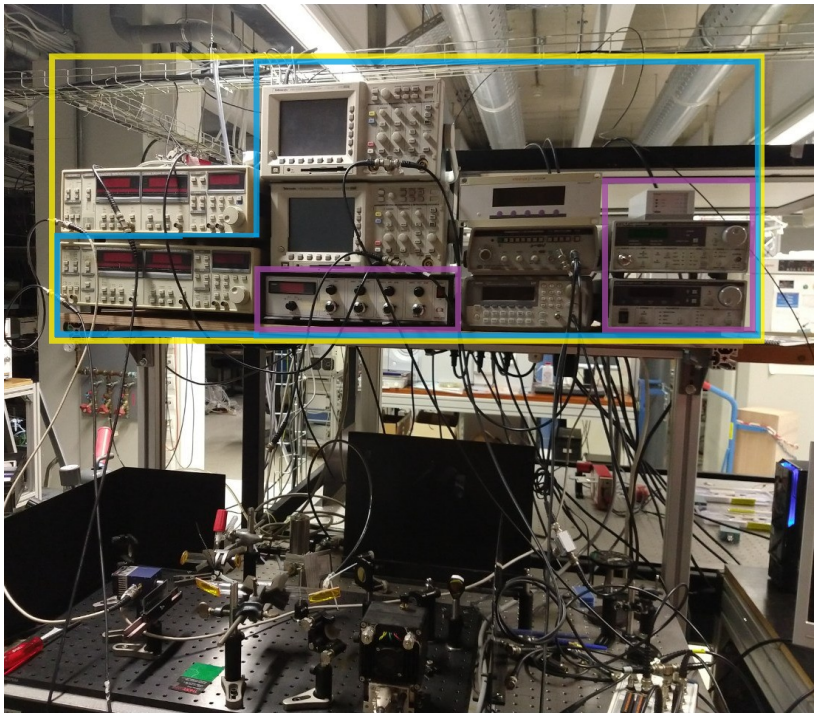

Figure 10: The full WMS setup is built on a movable table. On the shelf, all necessary equipment is installed. The rectangles indicate for which of the three variations of the setup which devices were used. The cyan rectangle includes everything except for the second lock-in amplifier, and is for the first setup. The yellow rectangle indicates the whole stack for the simultaneous 2f/1f measurement. In the third variation, everything except for the detector amplifier, laser current drive, and laser temperature controller on the right, and the flow controller in the center, was removed. This is highlighted by the purple rectangle. On the table in the bottom of the photo, the optical setup is built.

Figure 11: The QCL as used in these experiments is a small M905I chip mounted inside a laser housing (between the A and K in the photo on the right). The chip is mounted against a Peltier element to control its temperature. The back of the housing is a large heat sink. In front of the laser, an adjustable diaphragm with a lens is placed (front cover on the left).

2.1 Single lock-in amplifier

At a heat sink temperature of 33.0 °C and a direct drive current of 450 mA, the laser emits at a center wavelength of 4.61 µm (the equivalent of wavenumber 2169.2 cm^{-1}). It is driven by a laser current driver (LDX-3232, ILX Lightwave) that mixes the direct current with the scanning and modulation signals. The scan is a half duty cycle sawtooth wave of amplitude 3.72 mA (0.82 % of the direct current) at 15.4 Hz (generated by a GFG-8015G, GW Instek). The modulation is performed by a sine wave of amplitude 2.40 mA (0.53 % of the direct current) at 45.0 kHz (generated by a 33210A, Agilent). The current source translates the input voltage to a modulation current with a factor 200 $\frac{mA}{V}$. Their respective outputs, as well as the mixed signal, are confirmed by an oscilloscope (TDS 3032B, Tektronix).

Superimposing a scanning current on the injection current of the laser allows us to cover the absorption feature of interest, the ro-vibrational transition of CO at 2169.50 cm^{-1}, as setting the center laser wavelength to exactly the center of the absorption feature is impossible. The laser chip is mounted in a Peltier element controlled, air cooled housing (modified LDM-4872, ILX Lightwave). At a supply current of 450 mA and held steady at 33.0 °C by a temperature controller (LDT-5980, ILX Lightwave), the laser outputs around 20 mW of optical power.

At the output of the laser housing, the beam first passes a collimating aspherical lens (f = 4 mm, NA = 0.56). The beam is then split using a beam splitter (BP145B4, Thorlabs) that reflects 45 % of the beam into the sample cell. The remaining 55 % passes through and is directed through a reference cell. The reference cell contains a mixture of 100 ppmv CO and the rest N_2 at 100 mbar and is used to locate the absorption peak in each scan during setup. The pressure is kept low to get a narrow absorption line shape by decreasing Doppler broadening. The temperature in the lab is always roughly 21 °C. After the reference cell, the beam is detected by a photovoltaic detector (PVI-6, VIGO).

The other part of the beam is directed through a 20 cm long glass absorption gas cell with 1.5 cm radius ZnSe windows placed at Brewster angle with respect to the beam

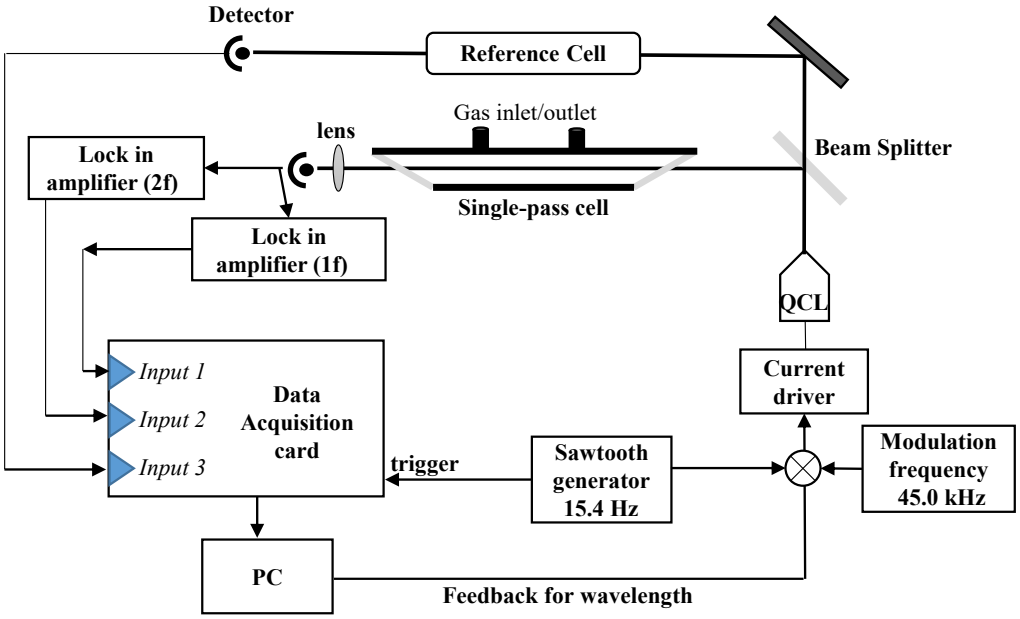

Figure 12: The QCL is driven by injection current $j(t)$ as described in equation (4). The beam is split and led through a sample cell and a reference cell, after which it is converted to an electrical signal that is further processed. [1, figure 2a]

path. This material and angle maximize transmission of the linearly polarized QCL beam through the windows. The sample cell has a volume of 35 mL. Finally, the beam is incident onto another photovoltaic detector (PVI-4TE-5, VIGO). This is a MIR thermo-electrically cooled single-point photodetector. As this detector is quite sensitive, the signal does not need to be focused. The total reduction of intensity from the output of the laser to the detectors was around 60% for both the reference and the sample paths, taking the beam splitter into account.

The sample detector signal is fed into the lock-in amplifier (SR830, Stanford Research Systems) to detect either the 1f or 2f harmonics. The time constant on the lock-in amplifier is set to 10 µs with a steep filter slope of 24 dB. This reduces oscillation in the signal without flattening the peaks. A parallel feed of the trigger signal of the sine wave generator is fed into the lock-in amplifier to synchronize the frequency. The phase between the generated sine and the detected signal can differ. A correction can be set on the lock-in to maximize the in-phase X signal, or just ignored if the total magnitude R is measured. When possible, the phase was corrected in these experiments. The lock-in simultaneously measured the in-phase X signal and its quadrature Y, thus it can output $R = \sqrt{X^2 + Y^2}$. In these experiments, the signal was tuned in-phase and the X output was measured.

In order to monitor the outputs, an oscilloscope (again a Tektronix TDS 3032B) is connected to the outputs of the oscilloscope and the trigger of the scanning wave generator. If all is right, a signal like in figure 8 (and in the results in figure 17) is seen (although probably a little less smooth).

Along with a triggering signal of the scanning signal, the 1f and 2f signals are connected to a DAQ interface (NI USB-6009, National Instruments). A self made LabVIEW program (see appendix A) collects the data at a sampling rate of 16 kHz. The data is

written to a plain text file to allow easy processing with other tools. The data acquisition rate is approximately 2 GB/h. The trigger signal is used to split the data into scans of the absorption feature. For each of these scans, the values of the 2f and 1f signals at $\omega_0 = \omega_L$ are found, that is the maximum peak height of the 2f signal and the 1f value at the same point in time.

2.2 Double lock-in amplifiers

After the repair of the laser, the optical power was reduced. At a temperature of 33.0 °C, driven by a direct drive current of 433.4 mA, the desired wavelength is reached. In order to still get good signal, the modulation depth was increased by doubling the amplitude of the sine to 9.6 mA (2.2 % of the direct current). As the optical power was reduced by a factor 100, the optical path was revised. After focusing by the lens in the laser housing, the beam is directed through the sample gas cell and directly incident onto the detector (PVI-4TE-5, VIGO). The signal is split to two lock-in amplifiers, one for extracting the 1f signal (SR844, Stanford Research Systems) and the other for the 2f signal (SR830). The data is acquired using the same LabVIEW program and DAQ interface as before. The location of the absorption feature can still be monitored by watching the 1f and 2f signals on the oscilloscope.

In the sample cell, a mixture of 100 ppmv of CO (remainder N_2) was kept at a steady pressure of 100 mbar by a pressure controller (EL-PRESS/EL-FLOW Prestige, Bronkhorst).

2.3 Measuring from LabVIEW

To enable easier data acquisition and reduction of needed devices, thus increasing portability and reproducibility, a new program was written in LabVIEW (by Ningwu Liu). The scanning and modulating signals are generated from the program, and output via the DAQ interface to the laser current driver. The raw signal from the photovoltaic detector is connected directly to the DAQ interface and input to the program. By using a higher sample rate DAQ (BNC-2110 connected to a PCIe-6341, National Instruments), these high frequencies can still be detected. The generated modulation signal was used as a reference to demodulate the input. The signal generator, lock-in amplifiers, and oscilloscopes were eventually removed from the setup. Monitoring, measuring, and some of the processing is now done in LabVIEW.

3 Results

3.1 Single lock-in amplifier stability

The first set of results comes from the initial setup as described in subsection 2.1. Example scans of the CO R6 transition are plotted in figure 13. These scans were performed with a full-duty sawtooth scan (i.e. symmetry in upwards and downwards slope). The absorption feature of interest lies near the edge of the scan, so not the whole shapes are visible, unfortunately. The 2f and 1f shapes are proportional to the second and first derivatives of the line shapes as expected. Comparing them to figure 8, the 2f signal seems flipped, thus the measured X signal was 180° out of phase with the reference. Although measurements of both the 2f and 1f signals were performed, they are incomparable as they were taken hours apart. Drift in the initial laser intensity I_0 is expected.

As the modulation depth was shallow, there is no significant offset in the 1f signal: the average seems to be zero. This means that the initial derivation of small modulation amplitude seems to hold.

For detecting the concentration of CO, most interest lies in peak values per scan. As simultaneous measurement of 1f and 2f signals was not possible at the time, we can take a look at the stability of the peak signal levels. A long measurement of the 1f and 2f signals (over two hours) was performed at a scanning frequency of 1.6 Hz. The minima and maxima are extracted. In figure 14, an Allan-Werle plot of these minima and maxima for the 1f and 2f scans is displayed. For increasing averaging time τ on the horizontal axis, the data is split into groups of length τ, thus in groups of 1.6τ samples. The average is taken for each group, and the mean deviation from this average is determined as σ_τ. Initially, as is expected, longer τ results in a smaller deviation. The decrease is mostly due to reduction of white noise and follows a line of slope $\tau^{-1/2}$ line. During this decrease, the environmental conditions might change, and causes a drift in the measurements. The laser intensity might change due to changes in lab temperature, for example. This results in an increase of the Allan deviation. After a certain τ, a

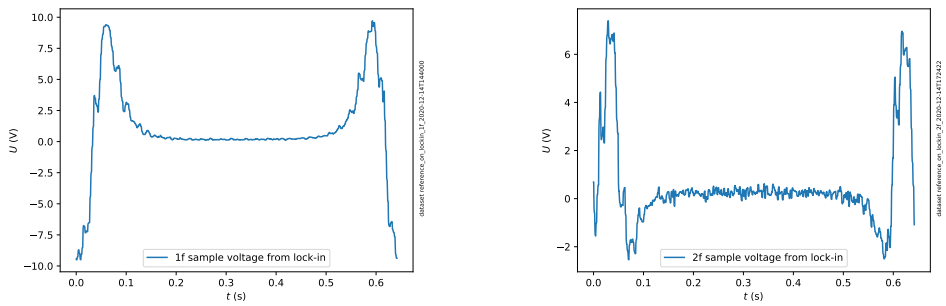

Figure 13: With a modulation frequency of 45.0 kHz and a full-duty sawtooth scan of 15.4 Hz, the lock-in amplifier outputs X values for the 1f and 2f signal similar to these two example scans. The coincidence of $\omega_0 = \omega_L$ is located around $t = 0.05$ s and $t = 0.65$ s. Do note that the scans are made some hours apart, and that normalization of the 2f signal by this 1f signal is therefore baseless.

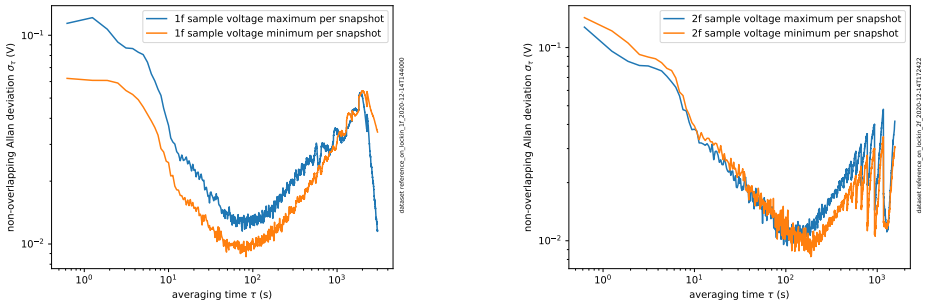

Figure 14: By collecting the 1f and 2f measurements of long measurement sets, and averaging them in increasingly larger groups, the displayed Allen-Werle deviation plots are produced. It is quite clear that averaging over 100 s *is optimal: flicker noise is reduced while minimizing drift. The measurements are of* 100 ppmv *of CO (remainder* N_2*) at* 100 mbar *in a cell of length* $\ell = 10$ cm.

minimum in the deviation is found. This is usually the optimal length of measurement. In our case, this is around 100 s. The 1 % minimal deviation from figure 14 implies a detection limit of around 1 ppmv.

3.2 Simultaneous 2f and 1f measurement

3.2.1 2f/1f WMS using two lock-in amplifiers

Now the setup is built according to subsection 2.2. The 2f and 1f signals are measured simultaneously. The cell contains 100 ppmv of CO at 100 mbar. To get optimal signal level, the modulation amplitude was doubled with respect to the initial setup. This value was determined by monitoring the 2f peak height while varying the modulation amplitude. The result can be seen in figure 15. It was decided to go with the maximum at 18 mV as to maximize the signal to noise ratio.

A measurement of half an hour at a scanning frequency of 7.45 Hz was taken, resulting in the measurement of 16786 scans of the absorption feature. An example scan of the 1f and 2f signals, and the 2f normalized 1f signal, is displayed in figure 16. Taking the average of all the scans results in figure 17. A phase shift of the 2f peak location and the 1f equilibrium crossing was observed in the measurement, as well as an offset in the 1f signal. The phase shift was due to the measurement of out of phase X values instead of R, and is corrected for. The small modulation approximation does not hold anymore. As was predicted, the offset is due to the small effect of absorption onto the 1f signal. This fact thus allows us to normalize the 2f. Afterwards, for every scan of the absorption feature, the 2f peaks are extracted, as well as the 1f values at these points in time. Their ratio is taken for all these values, and another Allan-Werle plot is produced (figure 18). The optimal measuring time seems to be 100 s. The mean absolute ratio of 2f/1f peak values is 2.27, thus the relative minimal deviation is 0.44 %. Before this can be expressed in terms of deviation of concentration measurement, a calibration has to be performed. This is left for the last setup change. Assuming a linear relation to the concentration, however, an indication of a detection limit around 0.44 ppmv is implied.

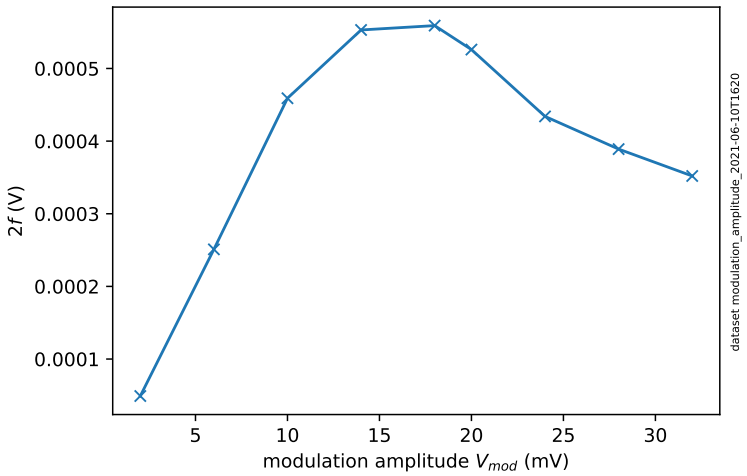

Figure 15: By increasing the modulation amplitude, a larger harmonic effect is achieved. The 2f peak height increases initially, but as the wavelength amplitude gets larger than the width of the absorption feature, the 2f peak decreases again. A maximum at 18 mV *was found.*

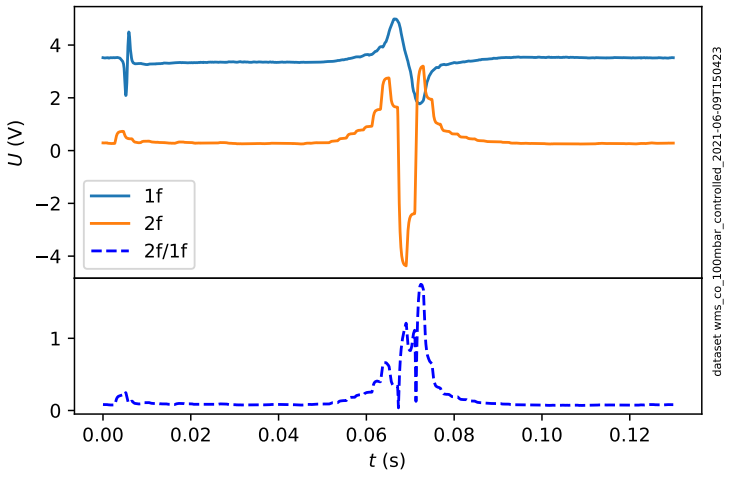

Figure 16: The 1f and 2f measurements of one scan of the absorption feature is shown. The phase difference between the 1f and 2f is corrected, and the 1f-normalized 2f is shown in the subplot below. The value of interest, is the value of the 2f/1f signal at the 2f minimum location.

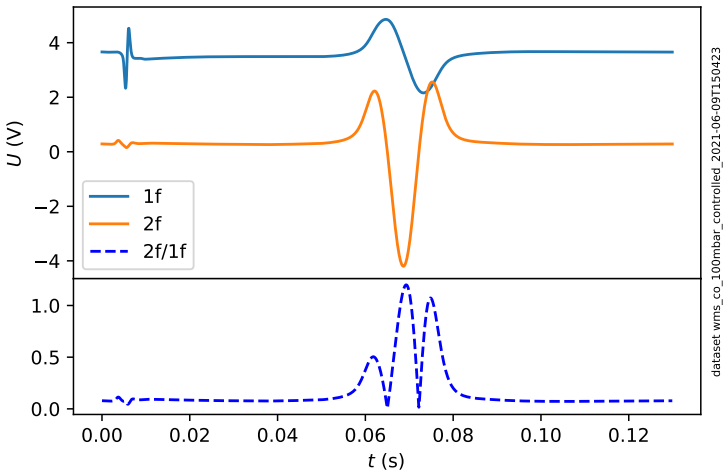

Figure 17: For the same measurement as in figure 16, the 1f-normalized 2f graph is calculated after averaging all scans. A height change of the middle 2f/1f peak with respect to the sample scan is observed.

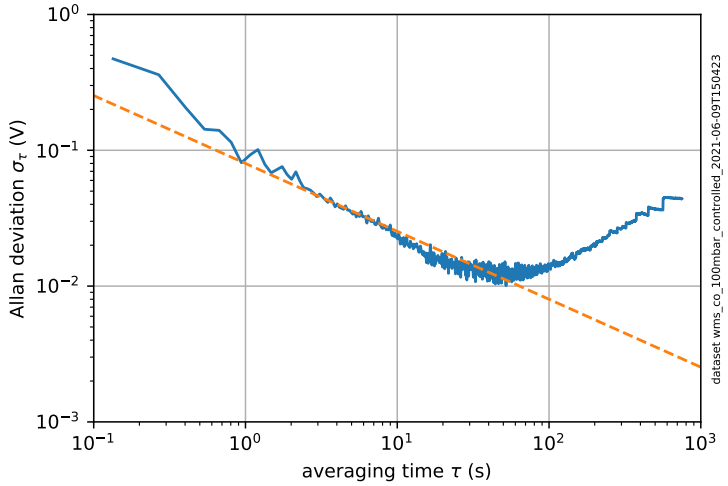

Figure 18: By taking the 2f/1f values at the 2f minimum location, the plotted Allan deviations are found.

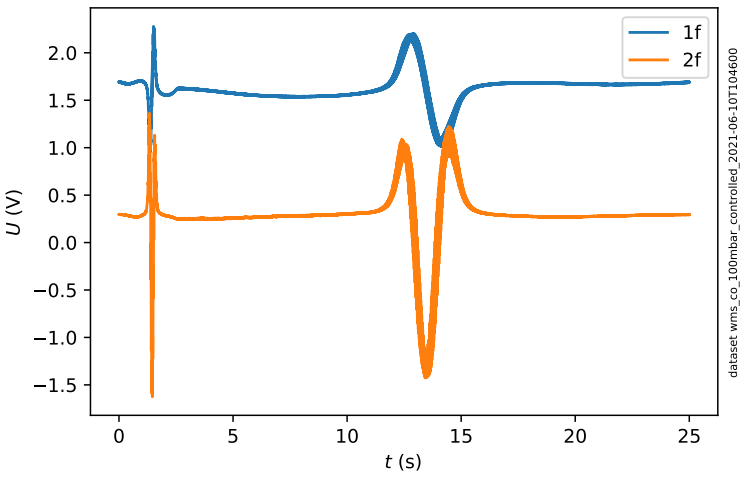

Figure 19: Using a scanning frequency of 0.04 Hz*, averaging all 23 scans results in the plotted graph. The drift in signal smears out the 1f and 2f shapes.*

3.2.2 2f/1f WMS from LabVIEW

Now the setup was compacted as was described in subsection 2.3. Another measurement at a slow scan frequency of 0.04 Hz was taken to illustrate the effect of drifts. The sample cell contained 100 mbar of 100 ppmv CO. The resulting average scan after almost ten minutes of measuring is displayed in figure 19. The Allan-Werle plots are omitted, as they are just rising lines.

Then the scanning frequency was changed to 100 Hz. This seemed slow enough to get a good resolution of the scan, and fast enough to measure no observable drift in the scan. A calibration of the setup was performed. A set of measurements of different concentrations of CO was done by dynamically mixing pure N_2 and 100 ppmv CO with two flow controllers. The result is displayed in figure 20. Although it is small, a background signal is observed as the intersect is not perfectly at the origin. This is probably due to CO absorption outside of the sample cell, electronic or optic impurities, or other small sources of EM radiation. A linear regression does result in a good fit ($R = 0.9990$). Now the setup is fully calibrated to measure CO concentrations.

To further support the hypothesis of a proportional relation of 2f/1f signal to the concentration independent of the initial laser intensity, a neutral density gradient filter was introduced to the beam path, thus reducing I_0 by a constant factor. The result was a non-altering magnitude of 2f/1f signal, although the lower signal made noise more problematic.

Lastly, the detected limit was determined. A 25 min long measurement of the 2f/1f values of a concentration of 20 ppmv was performed. Using the calibration line, the measured concentrations were determined. An Allan-Werle plot of these measurements is displayed in figure 21. There is a clear minimum in deviation at 100 s, giving a detection limit of around 20 ppbv. This is nearly on par with the previously found limit for the equivalent system (7 ppbv [1]).

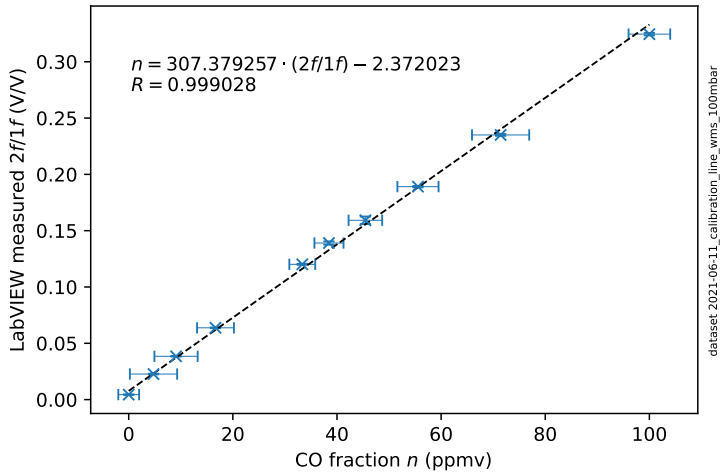

Figure 20: The system was calibrated by dynamically mixing N_2 and 100 ppmv CO. The error in adjustment of the flow was found as 1 % of the full scale of the flow controllers (5 L h^{-1}), thus the relative error increases with lower flows. The error in measured 2f/1f signal is drawn, but very small.

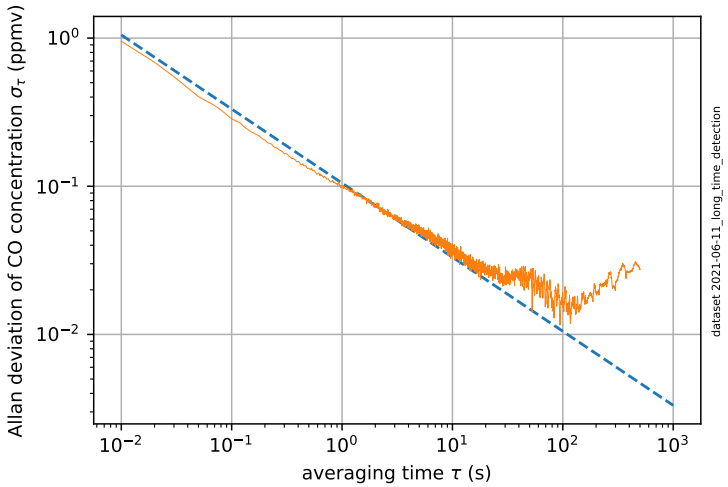

Figure 21: The Allan deviation minimum matches the previous results. It is found after 100 s of averaging and yields a detection limit of 20 ppbv.

4 Conclusion and outlook

During the internship, many different variations on the WMS setup were seen. The theory was tested and characteristics of the systems were described.

The theoretically predicted response of the 1f and 2f signals (equation (21)) seems to hold for shallow modulation depths. The shapes of the harmonic amplitudes show a response linear to the derivatives of the line shape function. By taking a look at the stability of the harmonic amplitudes at the coincidence of the laser wavelength with the center of the absorption feature, a minimum in deviation is established after 100 s. For large modulation depths, however, the effect of the absorption on the 1f shape was negligible, and the signal could be used for normalization of the 2f signal. This yields a system that can withstand variation in intensity due to absorption, deflection, intensity modulation, and other effects. The trade-off between minimizing drift and maximizing time resolution in the scan was explored, and an optimum in the range of 10 Hz to 100 Hz is found. The effect of interference of the harmonics of 50 Hz due to power supplies was only observed in the discrete lock-in amplifiers setup: the LabVIEW based setup seemed to reject this noise.

Finally, after calibration of the LabVIEW setup, a detection limit of 20 ppbv CO was achieved from a sample of 20 ppmv CO at 100 mbar. This is better than the estimated detection limit of the dual lock-in setup of around 0.44 ppmv. The stability remained the same, with an optimum after 100 s. This detection limit is enough for medical application (measurement of eCO of 1 ppmv to 5 ppmv). It can also be used for measurement in harsh conditions, like for monitoring CO after an electrical discharge (in plasma state). It is close to the detection limit found by the previous experiments performed in the Trace Gas Research group (7 ppbv [1]). The detection limit might be improved upon by taking into account the intensity modulation via a simulation fit (as was discussed in paragraph 1.5).

The choice between using the discrete hardware (lock-in amplifiers and signal generators) and doing all generation and processing in software depends on the situation. The discrete hardware can be more insightful to use, and is a good setup to learn from. The continuous resolution or high sample rates of modern discrete devices minimizes distortion. It is, however, a bit bulky and expensive to use all this hardware. Moreover, the long signal paths and combination of devices introduce more noise.

The LabVIEW setup has other benefits and problems. At lower resolution and low sample rates, distortion is introduced to the software generated signals. In data acquisition, higher harmonics may be undetectable if the sampling rate is too low. If the resolution is too coarse, small fluctuations in the harmonics are lost. The weakest link in the software approach is therefore the DAQ interface. Processing power will not be the bottleneck, nowadays. Having the signal generation and data processing both in software does allow for easy locking into the measured signal, and ease of use of the setup. Feedback to keep the absorption feature stable in frame is easier in this approach. I would therefore recommend going this route for practical use of WMS.

A look into the future of the technique gives two paths. The first might be further improving the sensitivity of the setup. This could for example be done by increasing the optical path length or initial laser intensity. The second is improving the accessibility and portability of the technique, which is already being explored by others [28].

5 Acknowledgments

I would like to thank the whole Trace Gas Research group for their help and company during my internship. It was a strange year due to COVID-19, but it was good to still be able to do work in the lab with others. The (not so) occasional help from Beate Stevens, Khalil Eslami Jahromi, Amir Khodabakhsh, Paul Assman, Nick Kersten, Ali Abbas, Roderik Krebbers, Ningwu Liu, Simona Cristescu, and Magda Speijers, whether it was in the lab or in the office, was much appreciated. They left a deep impression on my work, and my further (scientific) career. In particular, I would like to thank my supervisor, Frans Harren, for allowing me to do this research and supervising me along the way.

During the last week or so of the internship, Ningwu Liu and Roderik Krebbers helped me out a lot by getting the WMS setup to work after the repair of the laser for which I am very grateful.

Outside of the department, I am grateful for the times my girlfriend Marit listened to my chatter about WMS, harmonics, or just lasers in general. My father Jan and sister Anke also really helped by struggling through (the mathematics of) my thesis. There are others that helped me by listening, reading, and thinking with me, but are unlisted due to lack of space. Do know I am still grateful.

6 References

[1] Pakmanesh N, Cristescu SM, Ghorbanzadeh A, Harren FJM, Mandon J. Quantum cascade laser-based sensors for the detection of exhaled carbon monoxide. Applied Physics B. 2016 Jan;122(1):10. Available from: https://doi.org/10.1007/s00340-015-6294-7.

[2] Lawin H, Ayi Fanou L, Hinson V, Wanjiku J, Ukwaja NK, Gordon SB, et al. Exhaled carbon monoxide: a non-invasive biomarker of short-term exposure to outdoor air pollution. BMC Public Health. 2017 Dec;17(1):320. Available from: http://bmcpublichealth.biomedcentral.com/articles/10.1186/s12889-017-4243-6.

[3] Henderson B, Khodabakhsh A, Metsälä M, Ventrillard I, Schmidt FM, Romanini D, et al. Laser spectroscopy for breath analysis: towards clinical implementation. Applied Physics B. 2018 Aug;124(8):161. Available from: http://link.springer.com/10.1007/s00340-018-7030-x.

[4] Antuni JD. Increase in exhaled carbon monoxide during exacerbations of cystic fibrosis. Thorax. 2000 Feb;55(2):138–142. Available from: https://thorax.bmj.com/lookup/doi/10.1136/thorax.55.2.138.

[5] Snoeckx R, Bogaerts A. Plasma technology – a novel solution for CO_2 conversion? Chemical Society Reviews. 2017;46(19):5805–5863. Available from: http://xlink.rsc.org/?DOI=C6CS00066E.

[6] Goede A, van de Sanden R. CO_2 -Neutral Fuels. Europhysics News. 2016 May;47(3):22–26. Available from: http://www.europhysicsnews.org/10.1051/epn/2016304.

[7] Gordon IE, Rothman LS, Hill C, Kochanov RV, Tan Y, Bernath PF, et al. The HITRAN2016 molecular spectroscopic database. Journal of Quantitative Spectroscopy and Radiative Transfer. 2017 Dec;203:3–69. Available from: https://linkinghub.elsevier.com/retrieve/pii/S0022407317301073.

[8] Mina-Camilde N, Manzanares I C, Caballero JF. Molecular Constants of Carbon Monoxide at v = 0, 1, 2, and 3: A Vibrational Spectroscopy Experiment in Physical Chemistry. Journal of Chemical Education. 1996 Aug;73(8):804. Available from: https://pubs.acs.org/doi/abs/10.1021/ed073p804.

[9] Atoms, Molecules and Photons. Berlin/Heidelberg: Springer-Verlag; 2006. Available from: http://link.springer.com/10.1007/3-540-32346-5.

[10] Banwell CN. Fundamentals of molecular spectroscopy. 3rd ed. London ; New York: McGraw-Hill; 1983.

[11] Bradshaw JL, Bruno JD, Lascola KM, Leavitt RP, Pham JT, Towner FJ, et al. Small low-power consumption CO-sensor for post-fire cleanup aboard spacecraft. Orlando, Florida, United States; 2011. p. 80320D. Available from: https://sci-hub.se/10.1117/12.887517.

[12] Davis CC. Lasers and electro-optics. Cambridge: Cambridge University Press; 2014. OCLC: 878525359. Available from: https://doi.org/10.1017/CBO9781139016629.

[13] Centeno R. Advancing the detection of molecules in gas phase with infrared lasers: further development of semiconductor Laser-based Cavity Enhanced Absorption Spectroscopy [Ph.D. dissertation]. Radboud University. Nederland; 2015. OCLC: 959735076. Available from: https://hdl.handle.net/2066/150239.

[14] Nadeem F. Optical Re-Injection in Cavity-Enhanced Absorption Spectroscopy: Modeling and Experiments [Ph.D. dissertation]. Radboud University; 2020. Available from: https://repository.ubn.ru.nl/handle/2066/219233.

[15] Faist J, Capasso F, Sivco DL, Sirtori C, Hutchinson AL, Cho AY. Quantum Cascade Laser. Science. 1994 Apr;264(5158):553–556. Available from: https://www.sciencemag.org/lookup/doi/10.1126/science.264.5158.553.

[16] Schwaighofer A, Brandstetter M, Lendl B. Quantum cascade lasers (QCLs) in biomedical spectroscopy. Chemical Society Reviews. 2017;46(19):5903–5924. Available from: http://xlink.rsc.org/?DOI=C7CS00403F.

[17] Aellen T, Blaser S, Beck M, Hofstetter D, Faist J, Gini E. Continuous-wave distributed-feedback quantum-cascade lasers on a Peltier cooler. Applied Physics Letters. 2003 Sep;83(10):1929–1931. Available from: http://aip.scitation.org/doi/10.1063/1.1609044.

[18] Quantum Cascade Laser, 40 mW, CWL Between 4 and 5 µm; 2016. QTN010604-S01, Rev A. Available from: https://www.thorlabs.com/thorproduct.cfm?partnumber=QD4500CM1.

[19] Werle P. A review of recent advances in semiconductor laser based gas monitors. Spectrochimica Acta Part A: Molecular and Biomolecular Spectroscopy. 1998 Feb;54(2):197–236. Available from: https://linkinghub.elsevier.com/retrieve/pii/S1386142597002278.

[20] Rieker GB, Jeffries JB, Hanson RK. Calibration-free wavelength-modulation spectroscopy for measurements of gas temperature and concentration in harsh environments. Applied Optics. 2009 Oct;48(29):5546–5560. Available from: https://www.osapublishing.org/ao/abstract.cfm?uri=ao-48-29-5546.

[21] Kluczynski P, Axner O. Theoretical description based on Fourier analysis of wavelength-modulation spectrometry in terms of analytical and background signals. Applied Optics. 1999 Sep;38(27):5803. Available from: https://www.osapublishing.org/abstract.cfm?URI=ao-38-27-5803.

[22] Moeskops BWM. Spectroscopic detection of trace gases in the medical sciences [Ph.D. dissertation]. Radboud University; 2006. OCLC: 150297198. Available from: https://webdoc.ubn.ru.nl/mono/m/moeskops_b/specdeoft.pdf.

[23] Dávila J. Fourier description of lock-In. Revista mexicana de física E. 2013 06;59:1–7. Available from: https://www.researchgate.net/publication/262707506_Fourier_description_of_lock-In.

[24] Model SR830 DSP Lock-In Amplifier; 1992. Available from: https://www.thinksrs.com/downloads/pdfs/manuals/SR830m.pdf.

[25] Sun K, Chao X, Sur R, Goldenstein CS, Jeffries JB, Hanson RK. Analysis of calibration-free wavelength-scanned wavelength modulation spectroscopy for practical gas sensing using tunable diode lasers. Measurement Science and Technology. 2013 Dec;24(12):125203. Available from: https://iopscience.iop.org/article/10.1088/0957-0233/24/12/125203.

[26] Li H, Rieker GB, Liu X, Jeffries JB, Hanson RK. Extension of wavelength-modulation spectroscopy to large modulation depth for diode laser absorption measurements in high-pressure gases. Applied Optics. 2006 Feb;45(5):1052. Available from: https://www.osapublishing.org/abstract.cfm?URI=ao-45-5-1052.

[27] Liu N, Xu L, Zhou S, Zhang L, Li J. Soil respiration analysis using a mid-infrared quantum cascade laser and calibration-free WMS-based dual-gas sensor. Analyst. 2021 May;Available from: https://pubs.rsc.org/en/content/articlelanding/2021/an/d1an00503k.

[28] Gandhi V, Heda S, Anand R, Zarin A S, Upadhyay A, Chakraborty AL. A Raspberry Pi-based field-deployable tunable diode laser spectroscopy system for the detection of CO_2 at 2003.5 nm. In: 2015 International Conference on Microwave and Photonics (ICMAP). Dhanbad, India: IEEE; 2015. p. 1–2. Available from: https://ieeexplore.ieee.org/document/7408713.

A LabVIEW

The data acquisition in the hardware based setup was performed using a LabVIEW program. In the following figures (figures 22 and 23), the program schematic is shown.

The fully software driven setup is made by someone else, Ningwu Liu, and is therefore not shown. It applies the same principles as the lock-in amplifiers and generates the modulation and scanning signals.

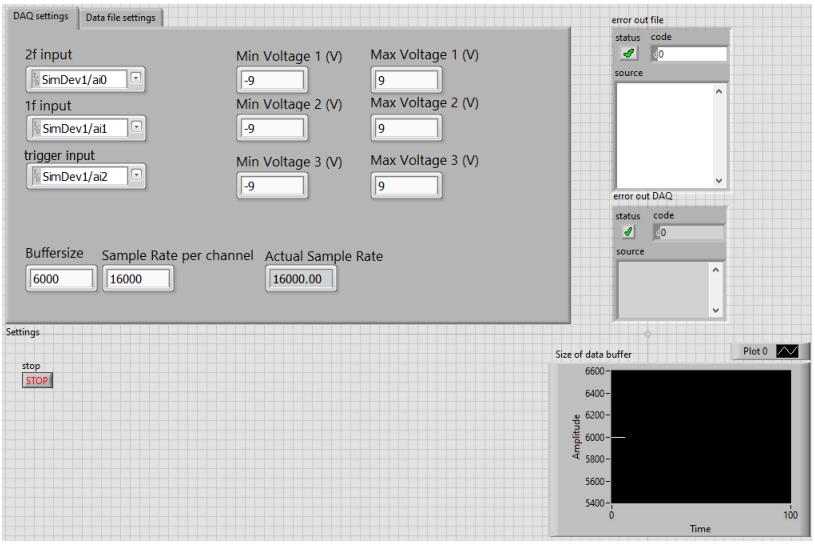

Figure 22: The settings for the measurement are put in on the front panel. This is also the place for online displaying of data.

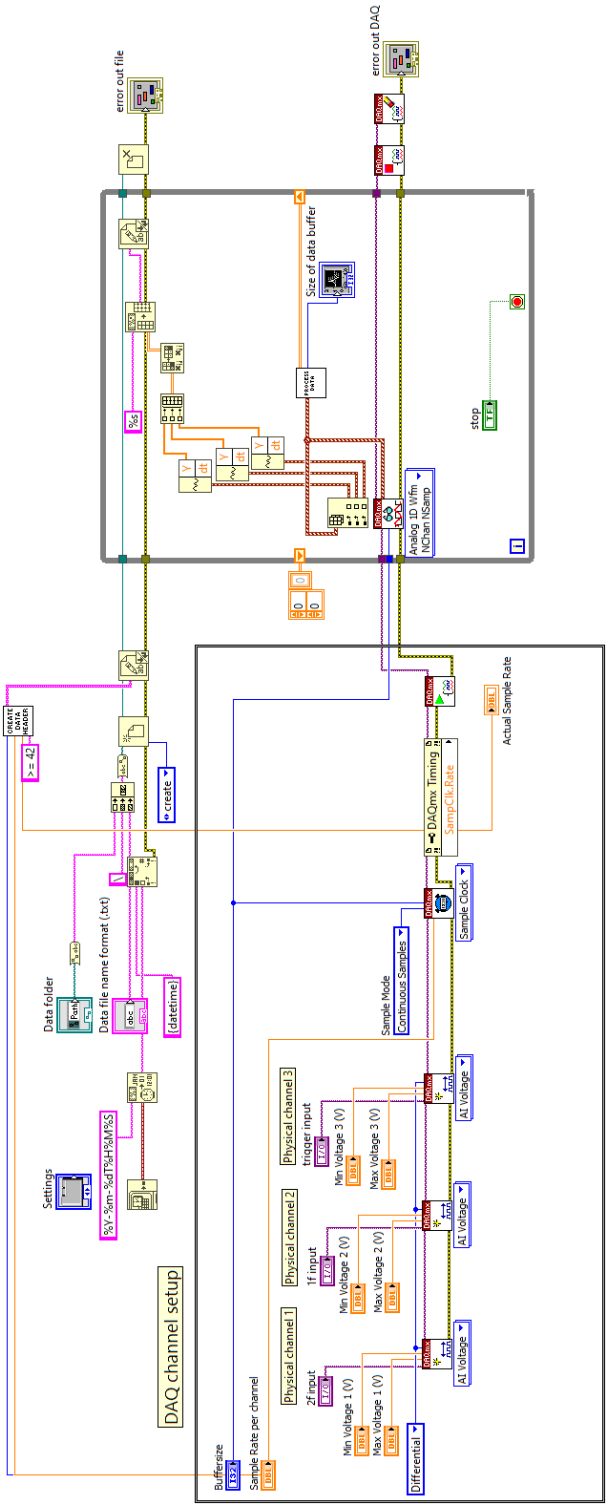

Figure 23: The LabVIEW program is programmed graphically by combining components in the block diagram. On the left, the setup for the DAQ interface is done. Above that, the settings and file name are handled. On the right, the measurement loop is displayed.